please cite the final published version as:

Y. Olivier, L. Muccioli, C. Zannoni, ChemPhysChem, 15, 1345–1355 (2014)

Quinquephenyl: the simplest rigid rod-like nematic liquid crystal. Or is it? An atomistic simulation.

Yoann Olivier[a], Luca Muccioli[b], and Claudio Zannoni[b]*

Abstract

We have performed an atomistic molecular dynamics study on the molecular organization and liquid-crystalline properties of quinquephenyl (P5), a prototypical mesogen and a molecule of interest for organic electronic. The thermotropic behavior reveals different mesophases. When cooling down from the isotropic phase, we find a transition to nematic (≈715 K), then to a smectic S_A (≈657 K) and another smectic, S_A^X (≈642 K), before a crystalline phase is recovered (≈617 K). This phase sequence is compared with experimental findings. We describe the different phases in terms of their molecular organization, orientational and positional order parameters and pair distribution functions as well as of their dynamics properties. In particular we discuss the smectic phases, that have not yet been characterized experimentally. Analyzing the effective shape of P5, we conclude that its internal torsions and bending make it not as rigid as could have been expected.

Keywords

Atomistic molecular dynamics*, phase transitions*, oligophenyls, nematics, order parameters, molecular rigidity, flexibility

1 Introduction

One of the most important challenges in the molecular design of liquid crystals (LC) is that of relating a specific molecular structure to collective physical observables like morphologies, order parameters and phase transition temperatures. This task would seem a nearly desperate one, in view of the

0[a] Yoann Olivier, Laboratory for Chemistry of Novel Materials,University of Mons, Place du Parc 20, BE-7000 Mons, Belgium

0[b] Luca Muccioli, Claudio Zannoni, Dipartimento di Chimica Industriale "Toso Montanari" and INSTM, Università di Bologna, viale Risorgimento 4, 40136 Bologna, Italy, email: Claudio.Zannoni@unibo.it

variety of chemical species forming typical mesogenic molecules, the number of ways they can be connected, their internal flexibility and the ensuing difficulties in defining a realistic set of interactions. In total contrast with the complexity of this problem, it is striking that most textbook pictures [1] and a vast number of coarse grained computer simulations of LC [2] resort to the drastic simplification of representing elongated mesogenic molecules as simple rod-like rigid objects like spherocylinders or prolate ellipsoids. These minimalist type of models, with some further key assumptions on inter particle interactions are at the root of the Onsager [3–7] and Maier-Saupe [8–11] theories for LC and their transitions, the main tools for our understanding of these complex materials.

Thus in Onsager type theories, the particles are assumed to be hard objects, only endowed with purely repulsive, steric, interactions when the particles overlap, or zero otherwise. In the original theory [3], a system of N elongated spherocylinders, i.e. right cylinders of length L, capped with hemispheres of diameter D, is studied by minimizing its orientational free energy written as a functional of the one particle orientational distribution expanded at second virial level for a certain density $\rho \equiv N/V$. For sufficiently high length to breadth aspect ratios, $a = (L + D)/D$ the theory predicts a spontaneous first order transition from isotropic to nematic phase as the density increases. A standard way of comparing the predictions of any theory of nematics with experiments is via the second rank order parameter $\langle P_2 \rangle$, the most important element of the family of Legendre polynomial averages:

$$\langle P_L \rangle = \int_0^\pi \mathrm{d}\beta \sin\beta P_L(\cos\beta)\mathcal{P}(\cos\beta),\ L = 2, 4, \ldots \tag{1}$$

where $\mathcal{P}(\cos\beta)$ is the distribution of orientations between the molecular axis $\mathbf{u}$ and the director $\mathbf{n}$, i.e. $\cos\beta \equiv \mathbf{u}\cdot\mathbf{n}$. It is well known that Onsager theory predicts a value of $\langle P_2 \rangle$ at the nematic-isotropic transition: $\langle P_2 \rangle_{NI}^{Ons} \approx 0.85$, and a entropy jump $\Delta S_{NI}^{Ons} \approx 8R$ much higher than experiment for most nematics [7, 12, 13].

The same system of hard spherocylinders has been studied in great detail by Frenkel and coworkers using Monte Carlo (MC) computer simulations [14]. Onsager theory can predict rather well the phase diagram of suspension of such hard rods with aspect ratio $a \gtrsim 10$, determined by simulations [14], or in experiments on viruses, nanorods and sufficiently long DNA sequences [15]. For shorter hard spherocylinders, simulations show [14] that for $a \lessapprox 4$ the

transition should go directly from isotropic to smectic, without an intervening nematic.

An alternative minimalist theory is the Maier-Saupe one, which in the original formulation considers attractive, van der Waals forces as dominating intermolecular interactions [8] and in a generalized form assumes that the pair potential, whatever its physical origin, can be expanded in a series of rotationally invariant functions of increasing rank [11]. In both cases in this type of theory the pair potential is converted, upon averaging over an isotropic distribution of distances and intermolecular vector directions, obviously a major assumption, to an effective, mean field orientational potential $U(\beta)$ acting on each individual molecule and determined self consistently. At second rank level $U(\beta)$ is proportional to the order parameter $\langle P_2 \rangle$ (or S as is often called [1]), thus

$$\langle P_2 \rangle = \int_0^\pi \mathrm{d}\beta \sin\beta P_2(\cos\beta) \exp[a_2 P_2(\cos\beta)]/Z. \qquad (2)$$

where $a_2 \equiv \bar{\epsilon}\langle P_2 \rangle / k_B T$ is a parameter expressing the strength of the anisotropic molecular field at temperature T and the pseudo-partition function Z ensures normalization. The order at the transition is $\langle P_2 \rangle_{NI}^{MS}$=0.43, independent on length or aspect ratio, much more similar to experimental values for low molar mass thermotropics. Given that most mesogenic molecules are non rigid, have flexible chains, dipoles, or other specific moieties it is surprising that these theories work relatively well in one or other respect. Since many drastic approximations are introduced in each theory, the agreement, where it exists, could be a result of cancellation of terms. For instance allowing in Mean Field theory for higher rank terms [10] or molecular biaxiality [16] could move the value of $\langle P_2 \rangle_{NI}$ up or down.

To compare theory and experiment, an ideal, simple, rigid and symmetric molecule would be highly desirable. As vigorously pointed out by Samulski and collaborators [17], para-quinquephenyl (PPPPP or P5) seems as close as possible to such a molecule. "If ever there were a calamitic mesogen that corresponded to the approximations used to derive S, the rod-like thermotropic LC PPPPP [...] is one among them." Studying such a molecule without major approximations, such as those introduced in simple statistical mechanics treatments would be highly desirable, e.g. to help clarifying the role of flexible chains or polar groups, here absent, or of the aspect ratio in determining nematic behaviour. Unfortunately P5 is a difficult system to study experimentally, in view of its high transition temperature and of

the possibility of chemical decomposition [18], and there is still a lack of general consensus even on basic things like the sequence of phases observed when cooling from isotropic down to crystal and the value of the clearing temperature [17, 19–23]. A realistic computer simulation of P5 is also not trivial [24], in view of the number of atoms in the molecule and the need to consider internal rotations of the rings and more generally to optimize the intramolecular and intermolecular contribution to the Force Field (FF) so as to obtain a reasonable reproduction of the phase transition [25].

Interestingly, quinquephenyl and more generally polyphenyl derivatives have also been for a long time prototype molecules for organic electronics, along with oligothiophenes [26, 27]. In particular, there is a considerable interest on these oligomers and their derivatives for their charge transporting properties [28] and for their use as model semiconductors for transistors [29] and as OLED [30]. Among the liquid crystalline ones, several derivatives have been synthesized with lower clearing temperature with respect to P5 [22, 31, 32]. In view of this multiplicity of interests, we wish to provide a simulation of quinquephenyl at full atomistic level of detail, developing a suitable FF, validating it and calculating liquid crystal properties as well as assessing its actual rigidity. We shall also discuss classical liquid crystal theories in the light of these results.

2 Results and discussion

2.1 Force field and Simulations

The first step in employing atomistic MD to study quinquephenyl and its phase behavior is the development of a properly tuned force field. Here partial atomic charges were computed by quantum chemistry techniques at the MP2//cc-pVDZ level of theory [33] with the ESP scheme [34], and inter-ring torsional potentials were evaluated at the same level of theory and introduced into an existing force field as customary [26]. We carried out Density Functional Theory and MP2 calculations, which consistently produced similar results for the two internal torsions, giving with a twist angle between the phenyl rings of about 40 degrees and energy barriers between 1.5 and 3 kcal/mol (see also Figure S1), and hinting the possibility of significant internal rotations at the high temperatures experimentally required to melt the material. Regarding the LJ parameters, preliminary tests on simulations

run in a cooling down sequence were carried out on a sample of $N = 200$ molecules by adopting three existing parameterizations: AMBER-OPLS [35], CHARMM27 [36] and the one optimized by Sherrill and coworkers for benzene dimers on the basis of high level ab initio calculations [37]. As usual the scaling factors for 1-4 intramolecular interactions were set to 5/6 for electrostatic and to 1/2 for LJ ones [35]. Unfortunately, all these force fields gave unsatisfactory results in terms of phase diagram and density values, therefore we decided to empirically optimize the LJ interaction between aromatic carbons so as to match the experimental density at 660K in the nematic phase (see Figure 1 and SI Figure S2 for details). We found an optimal value ε_{C}=0.105 kcal/mol, together with the OPLS parameters r_{C}=1.908 Å for carbon and ε_{H}=0.015 kcal/mol, r_{H}=1.459 Å for hydrogen [38], and these were used in the molecular dynamics runs described here.

All the simulations were carried out with NAMD 2.8 [39] at constant atmospheric pressure and temperature, using Berendsen's barostat and thermostat [38]. Periodic boundary condition were employed, adopting a cutoff of 12 Å for evaluating the Lennard-Jones (LJ) interactions and a smooth particle mesh Ewald method for electrostatic interactions [40] with grid spacing of 1.2 Å. A sample of N=1000 molecules contained in an orthorhombic cell was studied in a series of cooling runs, starting from an isotropic configuration at T=750 K, and gradually decreasing the temperature down to T=600 K, with equilibration times of at least 50 ns and production times ranging from 40 to 70 ns. In a second, more limited, series of runs, a supercell of the P5 experimental crystal structure (ZZZNKU01.cif, available from Cambridge Crystallographic Structural Database [27]) containing 1408 molecules was simulated at 300, 400, 500 and 600 K to compare with the structure of the crystal phases obtained by cooling. Configurations were stored every 100 ps and all the observables were calculated with in-house developed analysis codes.

2.2 Phase characterization

2.2.1 Density

We plot in Figure 1 the mass density obtained as a function of temperature upon cooling down from the isotropic phase, together with available experimental data [41]. Our Force Field is tuned for the nematic phase and we see a good agreement with experiment at the control point (660 K) and in the nematic and isotropic phase, at least where experimental data are avail-

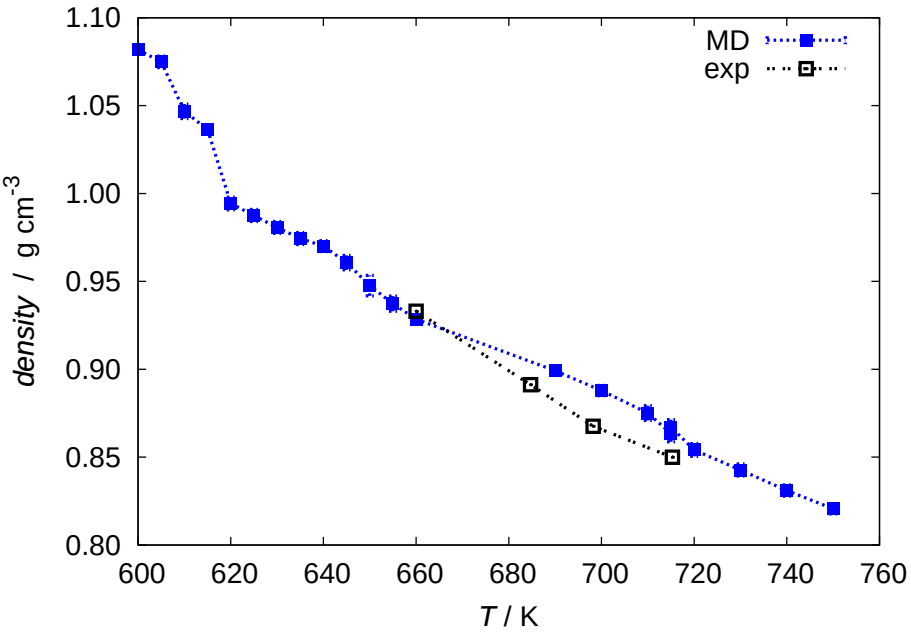

Figure 1: Comparison between simulated (full squares) and experimental (empty squares) [41] mass densities for quinquephenyl at various temperatures.

able [41]. Four phase transitions can be identified at $T \approx 715$, 657, 642, 617 K from changes of slope of the curve. In Figure 2 we show typical equilibrium snapshots of the molecular organizations obtained in the different phases, using a colour coding of the orientations. They show at once the disordered isotropic state (right) and on cooling down the onset of ordered phases that we shall now analyze.

2.2.2 Orientational order

The characterization of a liquid crystalline phase inevitably deals with the investigation of its orientational order with respect to the mesophase director. As this preferred orientation can fluctuate during the simulation, we determine the director $\mathbf{n}(t)$ at the successive time frames t considered in the MD trajectory as the eigenvector corresponding to the largest eigenvalue of

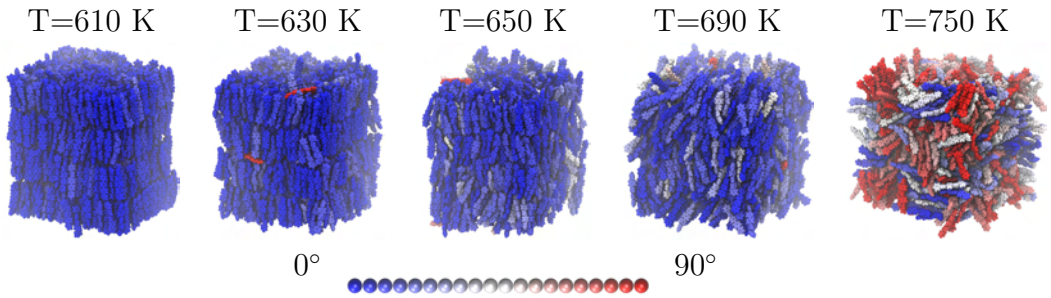

Figure 2: Typical molecular dynamics snapshots for the different phases, taken from the descending temperature sequence studied for P5. The color coding indicates orientations with respect to the director as from the palette.

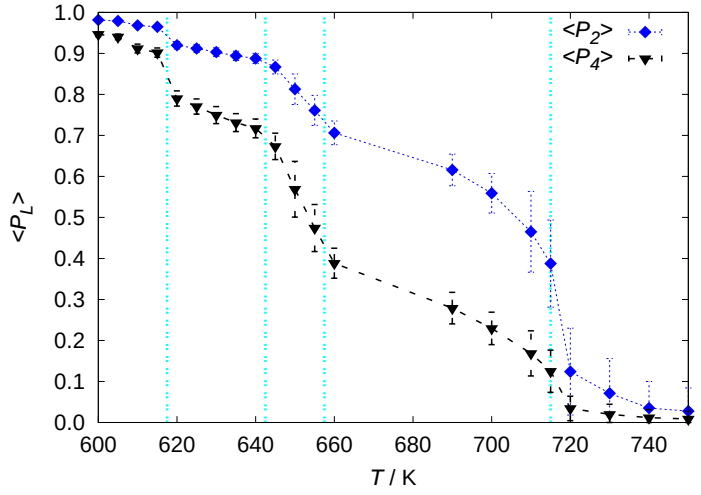

Figure 3: Second and fourth rank order parameters $\langle P_2 \rangle$ and $\langle P_4 \rangle$ vs temperature for P5 as obtained from MD. The vertical dashed lines indicate the estimated transition temperatures from present simulations.

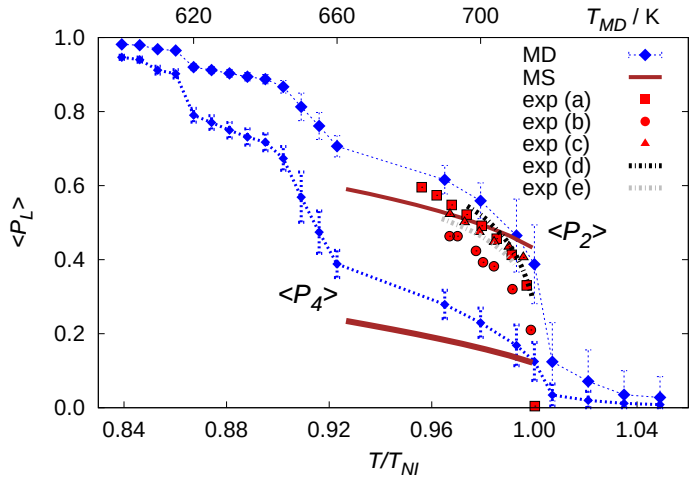

Figure 4: Average simulated order parameters $\langle P_2 \rangle$ and $\langle P_4 \rangle$ (filled blue symbols) for the long axis of P5 as a function of T/T_{NI}. We also report experimental values obtained from deuterium NMR by Dingemans et al. [17](a), from WAXS (b) and birefringence (c) by Kuiper et al. [42] and from two diamagnetic susceptivity anisotropy set of experiments by Sherrel and Crellin (d,e) [18]. The brown lines represent the Maier-Saupe mean field theory predictions for $\langle P_2 \rangle$ and $\langle P_4 \rangle$.

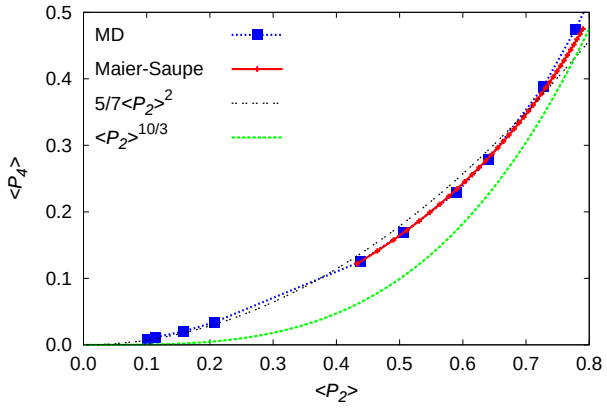

Figure 5: Simulated fourth vs second rank order parameters for P5 (blue symbols and dotted line as a guide for the eye). Maier-Saupe results (red continuous line), algebraic approximation [43] (black dotted line) and Faber theory [44, 45].

the ordering matrix, $\mathbf{Q}$ [25, 46, 47]:

$$\mathbf{Q}(t) = \sum_{j=1}^{N} \left[3\mathbf{u}_j(t) \otimes \mathbf{u}_j(t) - \mathbf{E}\right] / 2N, \tag{3}$$

where $\mathbf{u}_j(t)$ is the chosen molecular reference axis for molecule j; $\mathbf{E}$ is the identity matrix and the sum runs over all the N molecules of the sample. Here we chose as $\mathbf{u}_j(t)$ the principal axis of the inertia tensor for molecule j corresponding to the lowest eigenvalue. The instantaneous order parameter $P_2(t)$ can be obtained from the eigenvalues $\lambda_-(t) < \lambda_0(t) < \lambda_+(t)$ of $\mathbf{Q}(t)$. Here $P_2(t)$ is calculated as $P_2(t) = -2\lambda_0(t)$, as suggested by Eppenga and Frenkel [48]. The instantaneous eigenvalues of $\mathbf{Q}(t)$ are averaged over a sufficiently long and equilibrated trajectory, to give the scalar uniaxial order parameter as:

$$\langle P_2 \rangle \;=\; \langle P_2(t) \rangle \;=\; -2\langle \lambda_0(t) \rangle. \tag{4}$$

with the angular brackets indicating a time average over the trajectory. An alternative way of determining the order parameters employs the instantaneous director at time t, $\mathbf{n}(t)$ for computing the Euler angle $\beta_i(t)$ between the phase director and the reference axis of molecule i. This allows the calculation of the overall average of any function of β_i, and in particular, the

second and fourth rank Legendre polynomials, yielding the corresponding order parameters:

$$\langle P_2\rangle = \langle\sum_{i=1}^{N}(3\cos^2\beta_i(t)-1)\rangle/(2N), \quad (5)$$

$$\langle P_4\rangle = \langle\sum_{i=1}^{N}(35\cos^4\beta_i(t)-30\cos^2\beta_i(t)+3)\rangle/(8N). \quad (6)$$

where $\cos\beta_i(t) = \mathbf{n}(t)\cdot\mathbf{u}_i(t)$. We can now use these order parameters for a first assessment of the phase transitions observed in Figure 1. In Figure 3 we see that the highest temperature transition is a isotropic-ordered phase change. We shall see later that this higher temperature phase is devoid of positional order, confirming that the phase is nematic. Estimating T_{NI} from the simulations is not trivial, because of the finite and relatively small sample size that gives a non vanishing residual order even in the isotropic phase ($\gtrsim \sqrt{N}$) and the spacing between the temperature of our runs. Considering the highest temperature at which the inertial order parameter $\langle P_2\rangle$ is larger than 0.15, 715$\leq T_{NI} <$720 K. Some refinement can be obtained examining not only the average value of the order, but also the skewness of the histogram of all the instantaneous values of $\langle P_2\rangle$ observed during the simulation. The skewness of the order parameter is expected to become significant approaching a first order transition like the NI one [25, 43] and to change of sign crossing it, and as we see in the plot of skewness vs temperature reported in Figure S4, in our case this occurs around T=715 K, that we then use as our estimate of T_{NI}. Comparing with experiment we see that our simulations overestimate T_{NI} by ≈17 K (<3%). However it should be said that even the various experimental results differ from one another by even 5-7 degrees (see Table 1). In Figure 4 we show the simulated $\langle P_2\rangle$ and $\langle P_4\rangle$ vs reduced temperature. and compare them with available sets of experimental data for $\langle P_2\rangle$ while, as far as we are aware, experimental results are not yet available for $\langle P_4\rangle$. We notice that the agreement between simulation and experiment for $\langle P_2\rangle$ is good, both with the deuterium NMR data of Dingemans et al. [17], the diamagnetic susceptivity anisotropy measurements of Sherrel and Crellin [18] and the recent birifringence data of Kuipers et al. [42]. The wide angle X-ray data of [42] are more at variance both with our simulations and other experimental results.

Fitting our $\langle P_2\rangle$ results in the nematic phase to the empirical Haller equa-

Table 1: Quinquephenyl phase transitions as reported by various authors. Cr, S, N, I are short for crystal, smectic, nematic, isotropic. In brackets our proposed assignment for some previously observed transitions. The direction of the arrows distinguishes between heating and cooling runs.

Author	Phase sequence
Rodrigues et al. [23]	$Cr \xrightarrow{642K} S_A^X \xrightarrow{663K} N \xrightarrow{698K} I$
Kuiper et al. [42]	$Cr(S_A^X?) \xleftarrow{662K} S(S_A?) \xleftarrow{663K} N \xleftarrow{698K} I$
Dingemans et al. [17]	$Cr^1 \xleftrightarrow{623K} Cr^2(S_A^X?) \xleftrightarrow{663K} N \xleftrightarrow{700K} I$
Irvine et al. [19]	$Cr^1(S_A^X?) \xleftarrow{657K} Cr^2(S_A?) \xleftarrow{661K} N \xleftarrow{691K} I$
Irvine et al. [19]	$Cr(S_A^X?) \xrightarrow{663K} N \xrightarrow{698K} I$
Kuiper et al. [31]	$Cr(S_A^X?) \xleftarrow{658K} N \xleftarrow{692K} I$
Kuiper et al. [31]	$Cr(S_A^X?) \xrightarrow{666K} N \xrightarrow{699K} I$
present work	$Cr \xleftarrow{617K} S_A^X \xleftarrow{642K} S_A \xleftarrow{657K} N \xleftarrow{715K} I$

tion [49]:

$$\langle P_2 \rangle = (1 - \langle P_2 \rangle_{iso})(1 - T/T_{NI}^{\dagger})^{\beta_c} + \langle P_2 \rangle_{iso}, \tag{7}$$

with $T_{NI}^{\dagger}$=716 K, a pseudocritical temperature slightly above the first order transition T_{NI} and $\langle P_2 \rangle_{iso}$=0.12, gives a value of the pseudo–critical exponent β_c=0.18. This compares with those simulated for 5CB: β_c=0.226 $\pm$ 0.04 (for which the experimental values reported range from β_c=0.172 [50] to 0.19 [51] up to the value β_c=0.25 [52]. In Figure 5 we show a plot of $\langle P_4 \rangle$ vs $\langle P_2 \rangle$, where we see the simulated results compared with the Maier-Saupe expected curve and the simple approximation $\langle P_4 \rangle = (5/7)\langle P_2 \rangle^2$ [43] derived by eliminating the effective potential strength a_2 from the expressions in Equation 1 for L=2 and L=4, to obtain an expansion of $\langle P_4 \rangle$ in powers of $\langle P_2 \rangle$. The good agreement of the three curves essentially indicates that the orientational distribution has at each temperature a second rank exponential character, even if the temperature dependence of the effective field strength a_2 is not simply proportional to $\langle P_2 \rangle$ as in Maier-Saupe mean field theory. We notice that this should also apply to Onsager theories, since it is well known that the more complex expression for that can also be well represented by expanding the density functional form in its exponent in a Legendre poly-

nomial series truncated at the second term [5]. The other curve comes from the simple approximations $\langle P_4 \rangle = \langle P_2 \rangle^{(10/3)}$ continuum theory of disordering by fluctuations, which appears instead not to correspond to the behaviour of this realistic system, similarly to what was already found for the simple Lebwohl-Lasher lattice model [43].

2.2.3 Smectic phases and positional order

As already mentioned we find, when cooling down from the nematic, that other orientationally ordered phases appear. It is apparent from the snapshots in Figure 2 that these have a periodic structure, with molecules essentially orthogonal to the layers, suggesting that they could be smectics (thus, e.g. S_A or S_B) or crystalline. Various transitions have indeed been observed experimentally, but the situation is rather confusing (see Table 1). To characterize the phases we start by calculating their positional order parameters τ_n [26]. These represent the coefficients in the orthogonal expansion in a Fourier basis of the probability $P(z)$ of finding a molecule at a position z along the normal to the layers:

$$\mathcal{P}(z) = \frac{1}{d} + \frac{2}{d} \sum_{n=1}^{\infty} \tau_n \cos(2\pi n z/d) \tag{8}$$

where d is the layer spacing and we have assumed the origin of the director frame to be such that $\mathcal{P}(z) = \mathcal{P}(-z)$. τ_n, the nth positional order parameter, is defined as:

$$\tau_n = \int_0^d \mathcal{P}(z) \cos(2\pi n z/d)\, \mathrm{d}z = \langle \cos(2\pi n z/d) \rangle, n \geq 1 \tag{9}$$

In Figure 6 we show the first three positional order parameters obtained from our MD trajectories. Various methods to calculate τ_n and a robust procedure for their practical evaluation have been described in [53]. Here we have obtained the first few τ_n from a fit of the translationally invariant two particle density autocorrelation $g(z_{12})$, obtained from the number density of molecules at distance z_{12} scaled by the average density.

$$g(z_{12}) = 1 + 2 \sum_{n=1}^{\infty} (\tau_n)^2 \cos(2\pi n z_{12}/d) \tag{10}$$

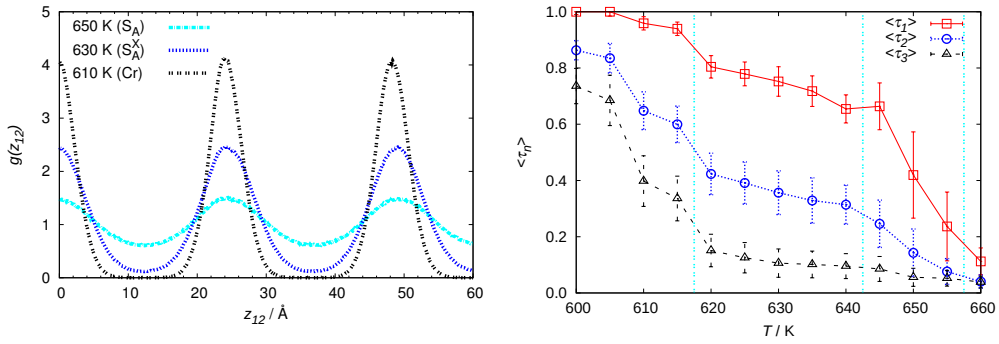

Figure 6: Typical oscillatory behaviour in the crystal and smectic phases of the two-particle density correlation function $g(z_{12})$ (left) and corresponding calculated positional parameters for P5 as a function of temperature (right).

The phase immediately below the nematic appears to be smectic with the first smectic order parameter τ_1 growing very quickly as T decreases below the nematic temperature range (Figure 6), in analogy to what observed for sexithiophene [26] but in contrast with other systems where it is instead rather constant in a similarly narrow temperature range [53]. The two low temperature phases are crystalline or smectic with high orientational ($\langle P_2 \rangle$ >0.9) and positional order. We notice also significant jumps in τ_2, τ_3 at the low temperature phase changes, showing a stiffening of the layers. The fit gives the simulated layer spacing as d =24.1-24.4 Å, similar to the value of almost 25 Å measured by Kuiper at al. [54] from the position of the X-Ray small angle diffuse reflection in nematic phase, and to the length of P5, indicating a non interdigitated organization, differently from, e.g. the case of 8CB [53].

2.3 Spatial and space-orientational distributions

We now take a closer look to the local structure of the phases, using first the radial distribution function:

$$g_0(r) \quad = \quad \frac{1}{4\pi r^2 \rho} \langle \delta(r - r_{ij}) \rangle_{ij}, \tag{11}$$

where $\mathbf{r}_{ij}$ is the distance vector between the reference centre on molecule i and the equivalent centre on molecule j and ρ is the number density. In Figure

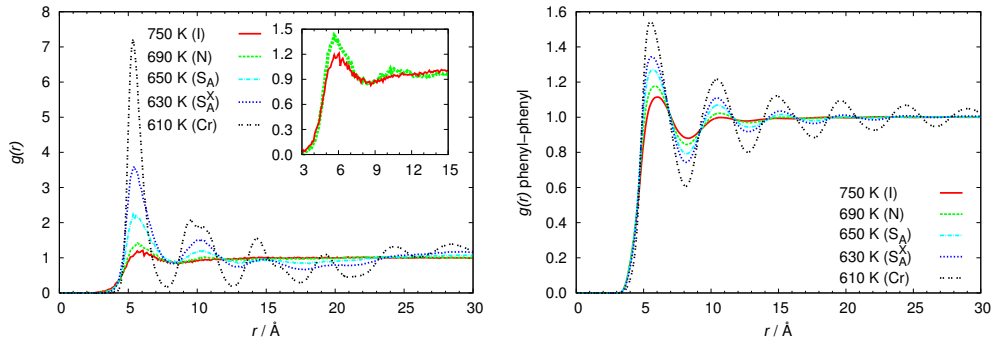

Figure 7: P5 radial distribution for centre of mass and inset of a close up across the NI transition (left) and radial distribution for centre of a phenyl ring with that of another phenyl ring (right).

7 (left) we show the radial distributions $g_0(r)$ of P5 in the nematic phase, obtained using as reference center the molecular center of mass. We see that $g_0(r)$ is liquid–like for the isotropic and nematic phase: no sharp peaks are present at medium and long range and g_0 quickly reaches the asymptotic value of 1, as expected for a fluid phase. We also notice that the isotropic and nematic correlations are quite similar even for temperatures well above the clearing temperature (see inset of Figure 7). In particular the first peak, shows the similarity in the local, short range, structure, hypothesized as the origin of the weak entropy change for the nematic-isotropic transition [13]. The radial distribution function also confirms the high structuring present in the two low temperature phases the crystalline and the lower tempearture smectic, that we shall tentatively call S_A^X, and the quantitative difference between those two. The first neighbour peak is located at 5-6 Å, rather than at $\approx$ 3.5 Å, as would be typically expected for face to face $\pi - \pi$ packing, corresponding to a local packing that is always somewhat skewed. This closest approach distance can be successfully compared with the value of 5.0 Å in the experimental crystal structure at room temperature. [27]. We also see that the our crystal phase has a local hexagonal structure, as shown by the splitting of the second peak of $g(r)$ [55] and the layer snapshots in Figure 8, while this feature is missing in the two upright smectic phases, that we can then tentatively classify as S_A, rather than S_B. We introduce next the pair distribution $G_2^{\alpha}(r)$, which gives the quadrupolar ordering between two

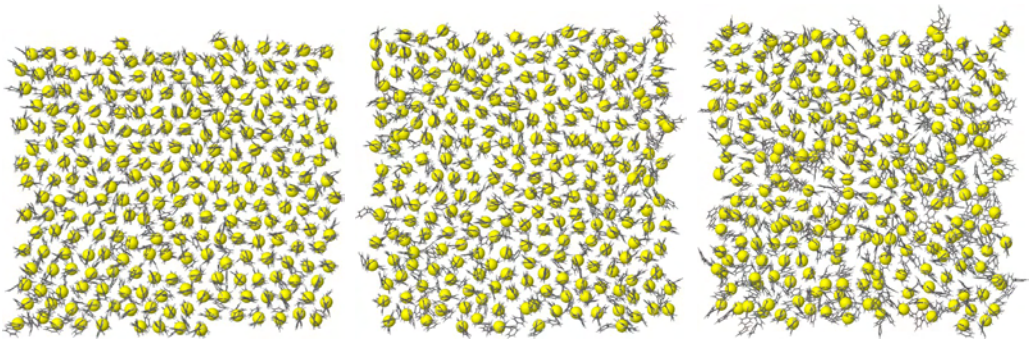

Figure 8: P5 wireframe top view of a layer in the crystal at 610 K (left), S_A^X at 630 K and S_A phases at 650 K. The spheres represent the centers of mass.

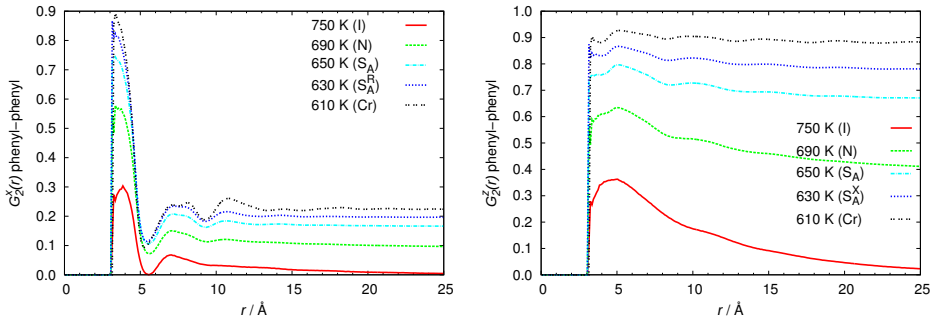

Figure 9: $G_2^\alpha(r)$ angular correlations for phenyl rings axes: along the P5 para direction (α=z, left) or perpendicular to it (α=x, right).

molecules i, j positioned at distance r,

$$G_2^\alpha(r) \quad = \quad \langle \delta(r - r_{ij}) \left[\frac{3}{2} (\mathbf{u}_i^\alpha \cdot \mathbf{u}_j^\alpha)^2 - \frac{1}{2} \right] \rangle_{ij} / \langle \delta(r - r_{ij}) \rangle, \qquad (12)$$

where $\mathbf{u}_i^\alpha$ is a reference unit vector in phenyl ring i, here along the P5 para axis (α=z) or perpendicular to it (α=x), and r is the distance between the reference centres on two different molecules. For P5 or oligophenyls in general, the relative orientation of the phenyl rings is of great importance as face to face orientation should favor the possibility of charge hopping from one molecule to the other, and thus improving its semiconducting properties. The correlation between two molecules is expected to be anisotropic and to vary when their separation vector $\mathbf{r}_{ij}$ is at different angles β with respect to the director. This can be examined with the anisotropic radial distribution

function, $g(r_{ij}, \cos\beta_{ij})$:

$$g(r_{ij}, \cos\beta_{ij}) = \frac{1}{4\pi r^2 \rho} \langle \delta(r - r_{ij}) \delta(\cos\beta - \cos\beta_{r_{ij}}) \rangle \ . \quad (13)$$

In practice, $g(r)$ of Equation 11 is calculated and normalized separately for discrete values of $\cos\beta_{r_{ij}}$, where $\beta_{r_{ij}}$ is the angle between the intermolecular vector r_{ij} and the phase director. In Figure 10 we report contour maps of $g(r_{ij}, \cos\beta_{ij})$ showing the molecular packing in various directions with respect to the director at various temperatures. We show a total of six cases and, to highlight significant differences, we choose a different scale for color coding the intensity of g for the three higher temperatures (0-2) and for the three lower ones (0-10). Starting from the isotropic phase just above the transition at 720 K, where the director is not really meaningful, we see that the distribution is essentially uniform and only shows short range order at $r_{ij} \approx 5$ Å while these local domains have nearly random orientation with respect to the pseudo-director. This local clustering is very similar to that at 710 K, just below the N-I transition. We see instead that the structure is very different, as we go through the various phase changes. The smectic A phase at 650K shows a pronounced correlation in the direction transversal to the director and, starting at ≈20 Å, with molecules of the neighbour layer. Cooling to 630 K shows an increase of the ordered region parallel to the director ($\cos\beta_{r_{ij}} \simeq 0$), but also the appearance of a second one with the intermolecular vector at $\approx 40^0$ from the first. After a further cooling and upon reaching the crystal a straightening seems to occur, with local and global ordering direction coinciding.

2.4 Dynamics

We still have to consider if the low temperature layered phases are smectic or crystalline, and examining their fluidity is useful in this respect. We have then calculated the translational diffusion coefficients along the director and perpendicular to it from the mean square displacements in the respective directions, using the classical Einstein formula (see, e.g. [53]). We see from the results in Figure 11 that the three high temperature phases are clearly fluid with translational diffusion coefficient of the order of 10^{-9} m^2/s, comparable with those of other nematics [56], of sexithiophene in the same high temperature range [26]. We see that both in the nematic and the smectic S_A phases the diffusion along the director is faster than the one perpendicular to it,

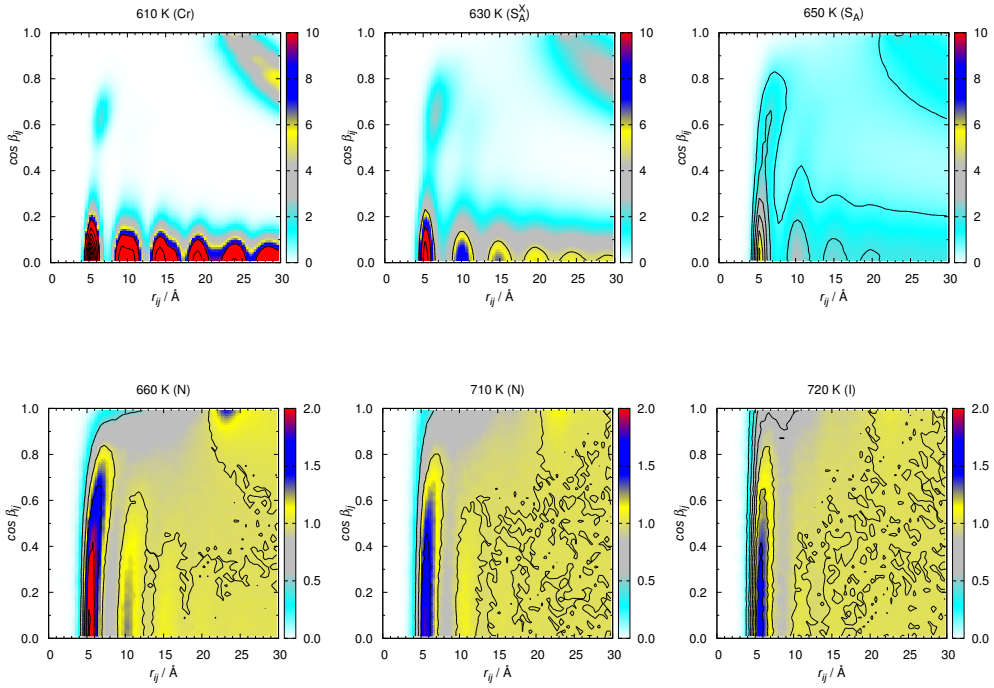

Figure 10: The distribution function $g(r_{ij}, \cos\beta_{ij})$ (equation 13) for P5 at a series of temperatures. β_{ij} is the angle between the director and the inter-particle vector $\mathbf{r}_{ij}$.

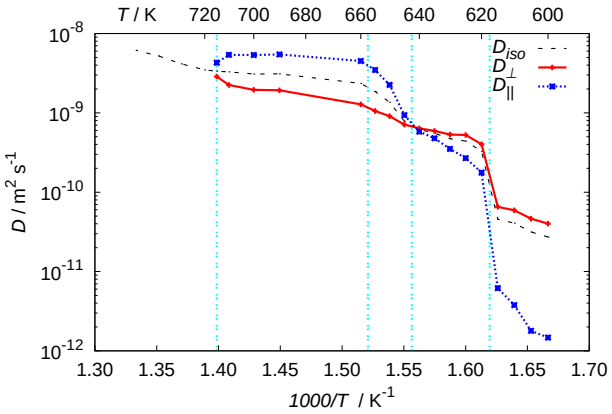

Figure 11: Arrhenius plot for the simulated translational diffusion coefficients of a P5 molecule moving parallel and perpendicular to the director.

again similarly to other systems where the nematic phase precedes the smectic one and the transition is of very weakly first or second order [26,53], or at temperatures close to the nematic-smectic transition in others [57]. This is somewhat surprising as the molecular flexibility is believed to play an important favorable role in interlayer diffusion [58], and hard spherocylinders with low aspect ratio show the opposite behavior with respect to P5 [59]. The translational diffusion becomes instead easier within the layers than across them in the low temperature smectic phase S_A^X, a feature typical of smectic phases with high interlayer energy barriers, such as tilted ones [57, 60]. In any case S_A^X retains some fluidity in both directions, qualifying it as a highly ordered smectic phase, rather than a conformationally disordered [21] crystal. Conversely in the Cr phase dynamics is slowed down by three orders of magnitude compared to the nematic and a (very slow) diffusion is possible almost only intralayer (the values of $D_{||} \approx 10^{-12}$ m^2/s reported correspond to an average root displacement of a few Å on the simulated timescale). As a matter of fact, this diffusion is compatible with the absence of spatial correlation between the layers both in S_A^X and in Cr at the temperatures we have studied (cf corresponding rdf in Figure S6). Apart from basic similarity, it is clear that we do not aim to reproduce the room temperature crystal polymorph by a cooling down process from the isotropic, a notoriously nearly impossible task [61, 62].

As for rotational diffusion, we have characterized it on the basis of the time-

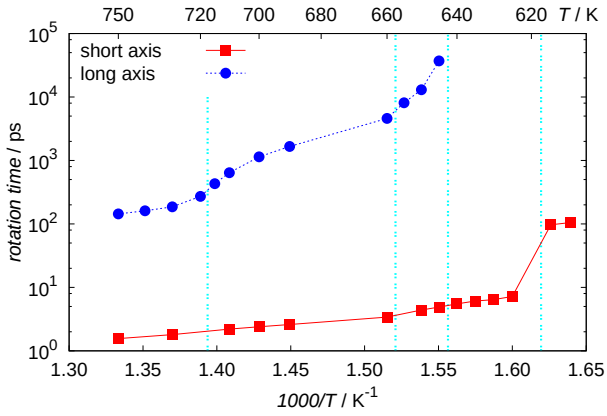

Figure 12: Arrhenius plot for the correlation times for rotation around the long axis (spinning) and of the long axis itself (tumbling) as a function of temperature.

autocorrelation functions $\langle \mathbf{u}(0) \cdot \mathbf{u}(t) \rangle$ where $\mathbf{u}$ denotes either the short or the long molecular axis of P5. These functions show a slow monotonic decay, and we arbitrarily estimated the corresponding characteristic time as the value at which $\langle \mathbf{u}(0) \cdot \mathbf{u}(t) \rangle = 1/e$. We see from Figure 12 that rotation around the long axis is fast (correlation times of the order of picoseconds) all the way from isotropic to smectic phases. Long axis reorientation starts instead from being two orders of magnitude slower than that of the short one in the isotropic phase, with a progressive increase of tumbling time, that becomes longer than 10 ns in the S_A^X phase and beyond our time window in the Cr phase.

2.4.1 Molecular Shape

The molecular shape, expressed by the aspect ratios between the molecular dimensions is a most important parameter in understanding LC phase behaviour, such as the onset of nematic and smectic uniaxial and biaxial phases, and the change in transition temperatures induced by small chemical modifications. Most of these effects have been widely studied in recent years with the help of hard [63] and attractive-repulsive rigid models [64]. More recently some of us proposed the use of deformable molecular models [65] to bridge the gap between a description that assumes mesogenic molecules to

be completely rigid or fully flexible. Among the shape effects on hard spherocylinders, a progressive increase of the length to breadth ratio is known to induce the nematic phase, widening it, and finally stabilizing a smectic phase [14]. To be more quantitative we consider, like in [25,47], the minimal rectangular box containing the molecule rotated in its inertial frame and its side lengths l_x, l_y, l_z as molecular size indicators. This molecule in a box approach provides an upper limit to the actual molecular dimensions, that on the other hand are difficult to define unambiguously for a non perfectly rigid molecule. In Figure 13 we show the temperature dependence of the average aspect ratio $\langle L/B \rangle$ obtained from molecular length $L = l_z$ and molecular breadth $B = (l_x + l_y)/2$, respectively. The histogram of the aspect ratio is not a sharp peak, independent of temperature, but rather we see a decrease of the average aspect ratio with temperature indicating non rigidity of the molecule. The non rigidity is also shown by the relatively broad distribution of L/B at various temperatures (Figure 13, right), somewhat similar to that of other more flexible mesogens [25, 66] and to sexithiophene [26]. The sources of the conformation changes leading to shape polydispersity in P5 appear to be quite different and involving mainly two mechanisms. One involves changes in the effective breadth of the molecule due to internal torsions while the length stays constant, with the phenyl-phenyl bonds parallel to the long axis of the molecules. In this sense the major changes with temperature occur on the short axis length (see Figure S8) yielding an intrinsic polydispersity which arises from the torsional degrees of freedom. The other mechanism is the presence of some overall bending of the molecule. As also shown by van der Schoot with a generalization of Onsager theory [67], allowing for even a small molecular flexibility stabilizes the nematic phase. Indeed, bending is actually a feature of P5 LC phases, as shown by the probability distributions of the cosine of the angle between the vectors joining the central phenyl with the two ends of the molecule, reported in Figure 14. The bending is also consistent with experimental measurements of persistence lengths of about 10-20 nm for rigid poly-para phenylene polymers in solution, values one order of magnitude larger of those expected for flexible polymers, but nevertheless quite small for a truly rigid one. [68, 69]. On the basis of simulation results for mono and polydisperse hard spherocylinders, this intrinsic polydispersity goes in the direction of explaining the wide nematic phase of P5, which is absent for aspect ratios lower than 4.7 for monodisperse hard spherocylinder systems [14] (Figure 15), while it is stabilized at the expenses of the smectic phase when flexibility [67] or polydispersity increases [70]. Actually

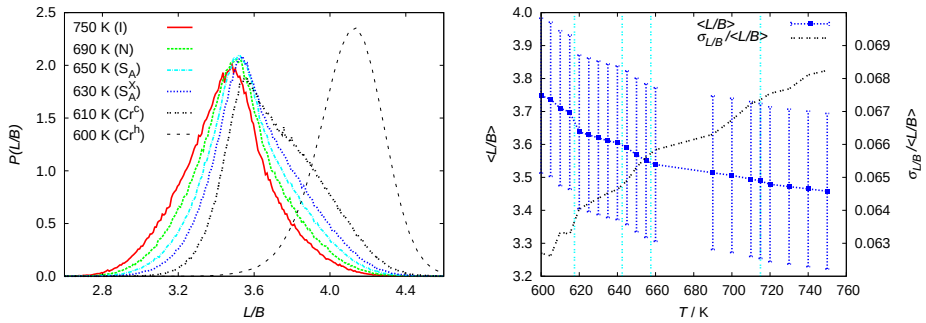

Figure 13: Left: distribution of the aspect ratio L/B as a function of temperature. Right: average aspect ratio, standard deviation and polydispersity.

polydispersity is also indicated as an important factor for obtaining smectic and nematic phases for colloidal systems with relatively low aspect ratio ($\simeq$ 4) [71]. Having said that, the other possible key element is the presence of anisotropic attractive forces for P5, missing in the hard particle models. We notice that the intervention of a purely scalar attractive dispersion force, as hypothesized in the so called van der Waals models [72, 73], goes in the right direction but still gives an overestimate of the order at the NI transition.

3 Conclusions

We have performed a detailed fully atomistic computer simulation of the molecular organization and phase transitions for p-quinquephenyl, a prototype rodlike mesogen. We have put forward a force field that can reproduce, upon cooling down from the isotropic phase, the transition temperature to nematic with a deviation of $\approx$17 K (<3%) from the experimental value. We also obtain two orthogonal smectic phases, with different anisotropy in the translational mobility of the molecules. In the higher temperature smectic phase molecules move more easily across the layers than in the layers, while the opposite is true in the lower temperature smectic one. It would seem that a combination of anisotropic dispersive and repulsive interactions is essential to give a liquid crystal, rather than just crystal phases for this relatively short aspect ratios and moreover that polydispersity in the aspect ratio, even for an apparently rigid molecule like P5 is important to yield a nematic, rather than a smectic. For P5 the polydispersity in shape and aspect ratio is pro-

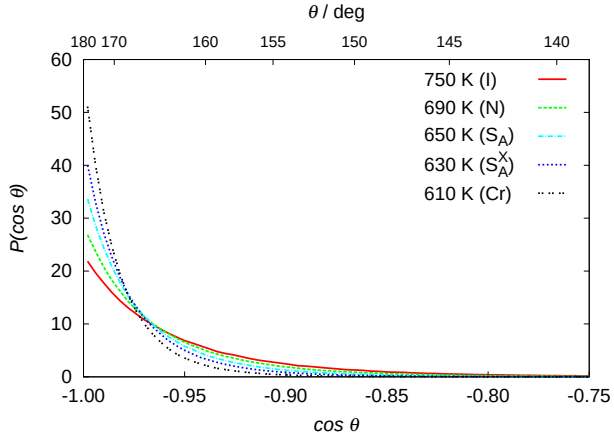

Figure 14: Probability distribution of bending for P5 at various temperatures. The bending angle θ is calculated between the para axis of the two phenyl groups PP at the two opposite ends of the P5 molecule (PP –P–PP).

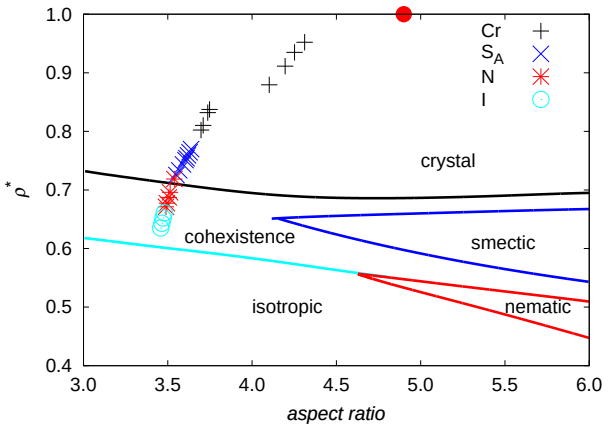

Figure 15: Comparison of atomistic simulation results with the reduced density versus aspect ratio phase diagram for hard spherocylinders as obtained by Frenkel and Bolhuis with Monte Carlo simulations [14]. The aspect ratio is defined as length over breadth, corresponding to $(L + D)/D$ in the usual notation for spherocylinders, while ρ^* is the reduced density expressed as fraction of the close-packed one ρ_{cp}. For scaling the atomistic data we used ρ_{cp}=1.292 g/cm^3, the density of the experimental crystal cell at room temperature. At the crystal geometry (ρ^*=1), the aspect ratio is 4.9 (r_x=3.5 Å, r_y= 6.6, r_z=24.6 Å), represented by the red circle in the phase diagram.

vided by internal torsions and bending. We have validated our results against existing data for transition temperatures and second rank order parameter as a function of temperature, but we have also predicted fourth rank orientational order parameter as well as positional order and diffusion coefficients that we hope will provide a stimulus for much needed further experimental work.

Acknowledgement

The work in Bologna has received funding from the MIUR PRIN national project "Novel ordered systems for high response molecular devices". Y. O. is a FNRS research fellowship and gratefully thanks EU HPC-Europa2 for funding his two research stays in Bologna and granting access to High Performance Computing resources at CINECA. C.Z. thanks Prof. Ed Samulski for stimulating discussions.

References

[1] P. G. de Gennes, J. Prost, *The Physics of Liquid Crystals*, Oxford U. P., 1993.

[2] C. Zannoni, *J. Mater. Chem.* **2001**, *11*, 2637-2646.

[3] L. Onsager, *Ann. N. Y. Acad. Sci.* **1949**, *51*, 627–659.

[4] K. Lakatos, *J. Stat. Phys.* **1970**, *2*, 121–136.

[5] G. Lasher, *J. Chem. Phys.* **1970**, *53*, 4141–4146.

[6] F. M. van der Kooij, K. Kassapidou, H. N. W. Lekkerkerker, *Nature* **2000**, *406*, 868.

[7] A. Khokhlov, in *Liquid Crystallinity in Polymers. Principles and Fundamental Properties*, (ed. A. Ciferri), VCH, 1991 pp. 97–129.

[8] W. Maier, A. Saupe, *Z. Naturforsch A* **1960**, *15*, 287.

[9] S. Chandrasekhar, *Liquid Crystals*, Cambridge University Press, 1992.

[10] R. Humphries, P. James, G. Luckhurst, *J. Chem. Soc. Faraday Trans.* **1972**, *68*, 1031–1044.

[11] G. Luckhurst, in *The Molecular Physics of Liquid Crystals*, (eds. G. Gray, G. Luckhurst), Academic Press, 1979 pp. 85–119.

[12] G. J. Vroege, H. N. W. Lekkerkerker, *Reports on Progress in Physics* **1992**, *55*, 1241, URL `http://stacks.iop.org/0034-4885/55/i=8/a=003`.

[13] G. Luckhurst, C. Zannoni, *Nature* **1977**, *267*, 412–414.

[14] P. Bolhuis, D. Frenkel, *J. Chem. Phys.* **1997**, *106*, 666–687.

[15] T. Bellini, R. Cerbino, G. Zanchetta, in *Liquid Crystals: Materials Design and Self-Assembly*, (ed. Tschierske, C), vol. 318 of *Topics in Current Chemistry*, Springer, 2012 pp. 225–279.

[16] G. Luckhurst, C. Zannoni, P. Nordio, U. Segre, *Mol. Phys.* **1975**, *30*, 1345–1358.

[17] T. Dingemans, L. Madsen, N. Zafiropoulos, W. Lin, E. Samulski, *Phil. Trans. Roy. Soc. (London) Ser.A* **2006**, *364*, 2681–2696.

[18] P. Sherrel, D. Crellin, *J. de Physique, Colloque C3* **1979**, *40*, 211–216.

[19] P. Irvine, P. Flory, *J. Chem. Soc. Faraday Trans. I* **1984**, *80*, 1821–1830.

[20] P. Irvine, D. Wu, P. Flory, *J. Chem. Soc. Faraday Trans. I* **1984**, *80*, 1795–1806.

[21] B. Wunderlich, *Thermochim. Acta* **1999**, *340-341*, 37–52.

[22] T. Dingemans, N. Murthy, E. Samulski, *J. Phys. Chem. B* **2001**, *105*, 8845–8860.

[23] A. S. M. C. Rodrigues, M. A. A. Rocha, L. M. N. B. F. Santos, *J. Chem. Thermodyn.* **2013**, *63*, 78-83.

[24] I. Cacelli, G. Cinacchi, C. Geloni, G. Prampolini, A. Tani, *Mol. Cryst. Liq. Cryst.* **2003**, *395*, 171–182.

[25] G. Tiberio, L. Muccioli, R. Berardi, C. Zannoni, *ChemPhysChem* **2009**, *10*, 125–136.

[26] A. Pizzirusso, M. Savini, L. Muccioli, C. Zannoni, *J. Mat. Chem.* **2011**, *21*, 125–133.

[27] K. Baker, A. Fratini, T. Resch, H. Knachel, W. Adams, E. Socci, B. Farmer, *Polymer* **1993**, *34*, 1571–1587.

[28] J. Kjelstrup-Hansen, J. E. Norton, D. A. da Silva Filho, J.-L. Brédas, H.-G. Rubahn, *Org. Electron.* **2009**, *10*, 1228-1234.

[29] G. Hlawacek, F. Khokhar, R. van Gastel, B. Poelsema, C. Teichert, *Nanolett.* **2011**, *11*, 333–337.

[30] A. C. Grimsdale, K. L. Chan, R. E. Martin, P. G. Jokisz, A. B. Holmes, *Chem. Rev.* **2009**, *109*, 897-1091.

[31] S. Kuiper, W. Jager, T. Dingemans, S. Picken, *Liq. Cryst.* **2009**, *36*, 389–396.

[32] N. Zafiropoulos, E.-J. Choi, T. Dingemans, W. Lin, E. Samulski, *Chem. Mater.* **2008**, *20*, 3821–3831.

[33] C. J. Cramer, *Essentials of Computational Chemistry. Theories and Models*, Wiley, 2004.

[34] B. H. Besler, K. M. Merz Jr, P. A. Kollman, *J. Comput. Chem.* **1990**, *11*, 431-439.

[35] W. L. Jorgensen, D. S. Maxwell, J. Tirado-Rives, *J. Am. Chem. Soc.* **1996**, *118*, 11225–11236.

[36] N. Foloppe, A. MacKerell, *J.Computat. Chem.* **2000**, *21*, 86–104.

[37] C. Sherrill, B. Sumpter, M. Sinnokrot, M. Marshall, E. Hohenstein, R. Walker, I. Gould, *J.Computat. Chem.* **2009**, *30*, 2187–2193.

[38] H. J. C. Berendsen, J. P. M. Postma, A. D. Nola, J. R. Haak, *J. Chem. Phys.* **1984**, *81*, 3684-3690.

[39] J. Phillips, R. Braun, W. Wang, J. Gumbart, E. Tajkhorshid, E. Villa, C. Chipot, R. Skeel, L. Kale, K. Schulten, *J. Computat. Chem.* **2005**, *26*, 1781–1802.

[40] U. Essmann, L. Perera, M. L. Berkowitz, T. A. Darden, H. Lee, L. G. Pedersen, *J. Chem. Phys.* **1995**, *101*, 8577-8593.

[41] A. Wuerflinger, M. Sandmann, in *Physical Properties of Liquid Crystals, Vol. 1: Nematics*, (eds. D. A. Dunmur, A. Fukuda, G. R. Luckhurst), IEE, London, 2001 p. 151.

[42] S. Kuiper, B. Norder, W. F. Jager, T. J. Dingemans, J. van Turnhout, S. J. Picken, *J. Phys. Chem. B* **2011**, *115*, 1416-1421.

[43] U. Fabbri, C. Zannoni, *Mol. Phys.* **1986**, *58*, 763-788.

[44] T. Faber, *Proc. Roy. Soc. London A* **1980**, *370*, 509–521.

[45] T. Faber, *Proc. Roy. Soc. London A* **1984**, *396*, 357–364.

[46] C. Zannoni, in *The Molecular Physics of Liquid Crystals*, (eds. G. R. Luckhurst, G. W. Gray), Academic Press, London, 1979 pp. 191–220.

[47] G. Tiberio, L. Muccioli, R. Berardi, C. Zannoni, *ChemPhysChem* **2004**, *5*, 104–111.

[48] R. Eppenga, D. Frenkel, *Mol. Phys.* **1984**, *52*, 1303-1334.

[49] I. Haller, *Prog. Solid State Chem.* **1975**, *10*, 103.

[50] S. T. Wu, R. J. Cox, *J. Appl. Phys.* **1988**, *64*, 821-826.

[51] R. G. Horn, *J. de Physique* **1978**, *39*, 105.

[52] I. Chirtoc, M. Chirtoc, C. Glorieux, J. Thoen, *Liq. Cryst.* **2004**, *31*, 229-240.

[53] M. Palermo, A. Pizzirusso, L. Muccioli, C. Zannoni, *J. Chem. Phys.* **2013**, *138*, 204901–204901.16.

[54] S. Kuiper, *Synthesis, Mesophase Behaviour and Charge Mobility of Phenyl-Thiophene Pentamers*, Ph. d., Technisch Universiteit Delft **2011**.

[55] R. Berardi, A. P. J. Emerson, C. Zannoni, *J. Chem. Soc. Faraday Trans.* **1993**, *89*, 4069.

[56] S. Miyajima, in *Physical Properties of Liquid Crystals: Nematics*, (eds. D. Dunmur, A. Fukuda, G. Luckhurst), vol. 25, INSPEC, IEE, 2001 pp. 457–463.

[57] M. Cifelli, G. Cinacchi, L. De Gaetani, *J. Chem. Phys.* **2006**, *125*, 164912.

[58] B. Mukherjee, C. Peter, K. Kremer, *Phys. Rev. E* **2013**, *88*, 010502.

[59] A. Patti, D. El Masri, R. van Roij, M. Dijkstra, *J. Chem. Phys.* **2010**, *132*, 224907.

[60] M. Cifelli, V. Domenici, S. Dvinskikh, C. Veracini, H. Zimmermann, *Phase Transitions* **2012**, *85*, 861–871.

[61] A. R. Oganov, *Modern Methods of Crystal Structure Prediction*, Wiley-VCH, 2010.

[62] A. Gavezzotti, *Cryst. Growth Des.* **2013**, *13*, 3801-3815.

[63] M. P. Allen, G. T. Evans, D. Frenkel, B. M. Mulder, in *Adv. Chem. Phys.*, vol. 86, Wiley-Interscience, 1993 p. 1.

[64] C. Zannoni, *J. Mater. Chem.* **2001**, *11*, 2637-2646.

[65] L. Muccioli, C. Zannoni, *Chem. Phys. Lett.* **2006**, *423*, 1-6.

[66] R. Berardi, L. Muccioli, C. Zannoni, *ChemPhysChem* **2004**, *5*, 104-111.

[67] P. van der Schoot, *J. Physique II* **1995**, *5*, 243.

[68] B. Farmer, B. Chapman, D. Dudis, W. Adams, *Polymer* **1993**, *34*, 1588-1601.

[69] S. Vanhee, R. Rulkens, U. Lehmann, C. Rosenauer, M. Schulze, W. Köhler, G. Wegner, *Macromolecules* **1996**, *29*, 5136-5142.

[70] M. A. Bates, D. Frenkel, *J. Chem. Phys.* **1998**, *109*, 6193.

[71] A. Kuijk, D. Byelov, A. Petukhov, A. van Blaaderen, A. Imhof, *Faraday Discussions* **2012**, *159*, 181–199.

[72] M. Cotter, in *The Molecular Physics of Liquid Crystals*, (eds. G. Luckhurst, G. Gray), Academic Press, 1979 pp. 181–189.

[73] W. Gelbart, B. Barboy, *Acc. Chem. Res.* **1980**, *13*, 290–296.

Table of content

Text

The nematic–isotropic and the other transition temperatures of p-quinquephenyl have been determined using atomistic molecular dynamics simulations. Various orientational and positional order parameters have been determined and compared with experimental data where available. The rigidity of p-quinquephenyl, often taken for granted is assessed, finding an aspect ratio changing with temperature and its distribution relatively broad due to internal torsion and bending.

Supporting Information

1 Parameterization of the force field

Taking into account the symmetry of para-quinquephenyl (P5), only two torsion angles along the para axis are to be reparametrized for obtaining an accurate force field, namely the outer torsion ϕ_1 and the inner torsion ϕ_2 (Figure S1). Similarly to other studies aiming at the calculations of biphenyl torsion potential [1], a batch of methods has been used ranging from the semi-empirical AM1, through hybrid DFT B3LYP and finally to MP2. Different basis sets with increasing size were used in order to rely as accurately as possible on minimum energy position as well as barrier heights. All the calculations were performed with Gaussian09 software [2].
From Figure S1, we can see that all the quantum-chemical methods (except B3LYP with the cc-pVTZ basis) converge to the same energy minimum around 40 degrees with a larger energy barrier at 0 degree than at 90 degrees for both torsion angles. We notice that the energy barriers at 0 and 90 degrees are quite similar with differences of the order of 0.2 kcal/mol. Interestingly, MP2 optimization and MP2 single point on B3LYP cc-pVTZ geometries give quite similar results, highlighting the predominance of the quantum-chemical method employed for calculating the energy over the one used for the geometries. Overall the results obtained in this study are in quite good agreement with previous calculations performed on shorter oligophenyls [3].
Prior to running molecular dynamics simulations, the torsional contribution

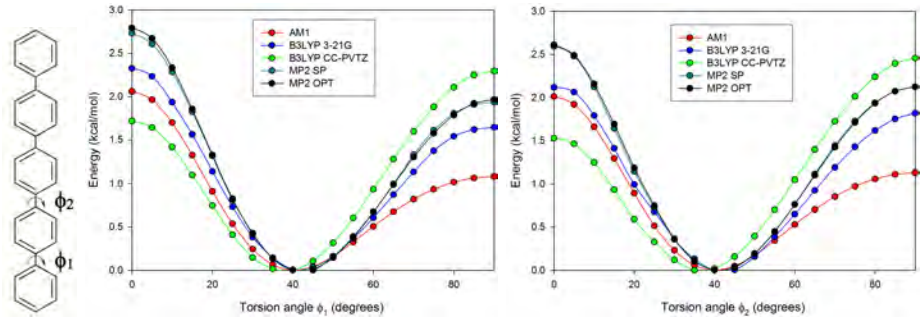

Figure S1: Quantum chemistry energy profiles for quinquephenyl dihedral angles Torsional potential for the outer torsion angle ϕ_1 and the inner torsion angle ϕ_2 of quinquephenyl, as shown in the chemical skectch on the left. The key MP2 OPT corresponds to MP2//CC-pVDZ calculations, while MP2 SP to B3LYP/cc-pVTZ/MP2/cc-pVDZ.

to the force field calculations were determined with the Adaptive Biasing Force (ABF) method as implemented in NAMD [4]. The best fit between ABF calculations and quantum-chemical calculations was then introduced in the force field definition. At the same time, the atomic charges were calculated using the ESP scheme [5] on the MP2//cc-pVDZ charge density, and symmetrized them with respect to the inversion center and introduced in the force field.
Preliminary Molecular Dynamics simulations on 200 molecules samples have been performed in order to assess the capability of the different parameteriza-

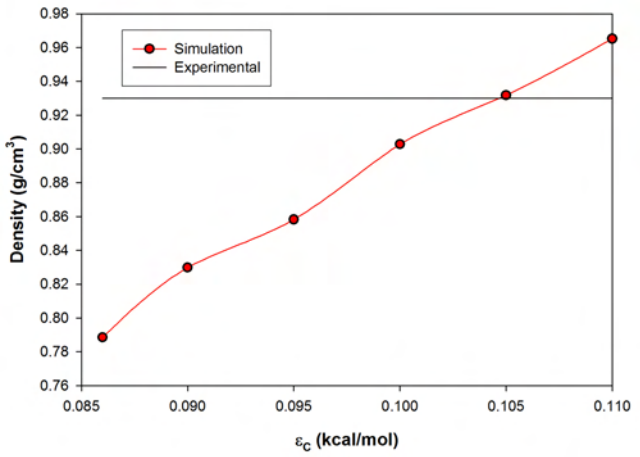

Figure S2: Density as a function of ϵ_C for an orthorhombic sample of 200 molecules at 660 K using the AMBER values for the remaining Lennard-Jones parameters (r_C=1.908 Å; ϵ_H=0.015 kcal/mol, r_H=1.459 Å [7])

tions for the Lennard Jones parameters reported in literature in reproducing the correct experimental density and transition temperatures. We instead kept the atomic charges fixed at their ab initio values and used as reference density the one of the nematic at the transition between crystal and liquid–crystalline (0.93 g/cm^3 at 660 K) [6]. The AMBER parameterization [7] (ϵ_C=0.086 kcal/mol, r_C=1.908 Å; ϵ_H=0.015 kcal/mol, r_H=1.459 Å) was our first natural choice since it has been used often in the Bologna laboratory, often obtaining a good agreement with experiments when torsional potential has been modified at a quantum-chemical level in addition with the introduction of ESP charges, see for instance reference [8]. However the density obtained with the AMBER parameterization is disappointingly lower than the experimental one (0.78 g/cm^3 at 660 K) also if at that temperature the sample is in the nematic phase; therefore we attempted also another popular force field, CHARMM (ϵ_C=0.07 kcal/mol, r_C=1.9924 Å; ϵ_H=0.022 kcal/mol, r_H=1.32 Å). The results with CHARMM were even worse: no stable condensed phase was obtained at atmospheric pressure in the simulated temperature range 600-720 K. In a third attempt, we recurred to the parameterization proposed by Sherrill and coworkers (ϵ_C=0.115 kcal/mol, r_C=1.922 Å; ϵ_H=0.011 kcal/mol, r_H=1.23 Å) [9] on the basis of high level, correlated calculations carried out for benzene dimers. This parameter set was supposed to perform better than existing ones, at least in reproducing the ab initio data: *"The new parameters lead to modest overbinding near equilibrium for the sandwich configuration, but they improve significantly the under binding of the empirical force fields for the T-shaped configuration."* [9] However our tests in condensed phase revealed this overbinding is detrimental for the liquid phase of quinquephenyl, as we obtained only solid phases and too high densities ranging from 1.07 to 1.21 g/cm^3 in the 600-720 K temperature range. From these tests it cleary emerged the key importance of tuning appropriately ϵ_C, together with the relatively superior performance of the AMBER force

Table S1: The different parameterization were furtherly tested also for supercells built by replicated the experimental crystal structure. Here we report density ρ and crystal cell parameters of quinquephenyl as obtained from X-ray experiments [10] and simulated for a 4 x 16 x 11 supercell.

	T (K)	ρ (g/cm^3)	a (Å)	b (Å)	c (Å)	β (°)
exp	283-303	1.29	22.056	5.581	8.07	97.9
ϵ_C=0.105	300	1.23	21.98	5.28	8.89	90[*]
ϵ_C=0.105	400	1.21	22.02	5.33	8.96	90[*]
ϵ_C=0.105	500	1.18	22.19	5.41	8.98	90[*]
ϵ_C=0.105	500	1.14	22.32	5.59	9.08	90[*]
ϵ_C=0.105	300	1.24	22.46	5.29	8.73	97.4
AMBER-OPLS	300	1.22	22.47	5.31	8.79	97.4
CHARMM	300	1.24	22.44	5.51	8.37	97.8
Sherrill	300	1.38	22.17	5.41	7.73	98.3

[*] β fixed to 90 degrees. α and γ are always fixed at 90 degrees.

field with respect to CHARMM and Sherrill's. On this basis, in a second series of simulations carried out at 660 K, we systematically increased ϵ_C from 0.086 kcal/mol, the original value in the AMBER parameterization, up to 0.11 kcal/mol (so somehow gradually transforming AMBER carbon in Sherrill's carbon), while leaving the other Lennard Jones parameters unchanged. As shown in figure S2, it turned out that ϵ_c=0.105 kcal/mol gave the density closest to the experimental value, and we employed this value for the simulations described in the article.

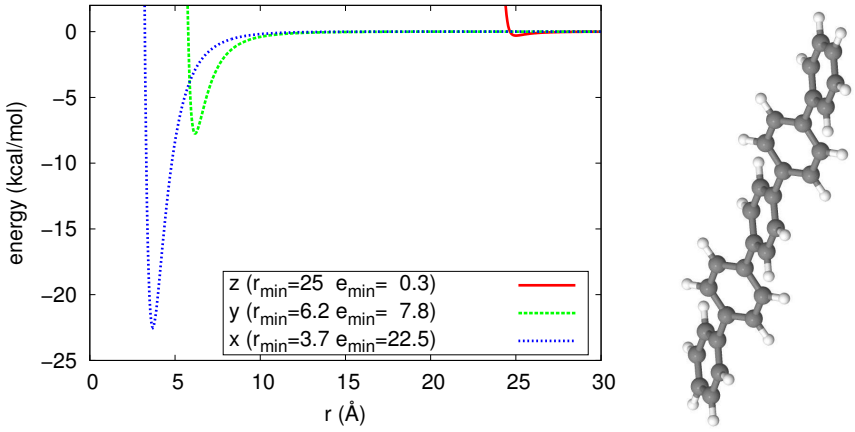

Figure S3: Potential energy curve for two parallel P5 molecules displaced along their principal inertia axes, calculated with ϵ_C=0.105 kcal/mol at the equilibrium geometry in gas phase (right). In the legend, the maximum interaction energies and the positions of the maxima are indicated. The positions provide also an estimation of the molecular dimensions and of the aspect ratio (in this case, $a = 2 \cdot 25/(6.2 + 3.7) \approx 5.06$).

2 Additional Figures

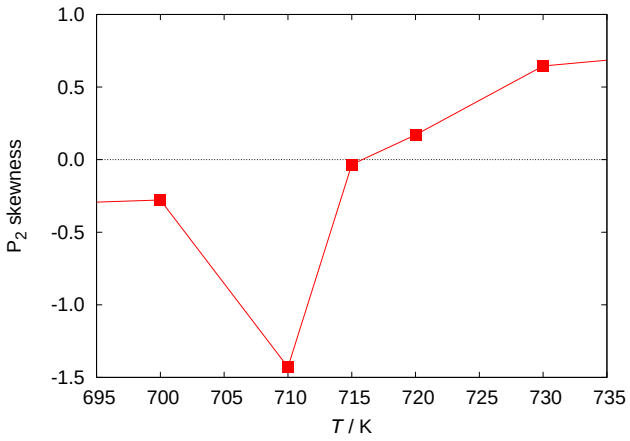

Figure S4: Skewness $\langle (P_2(t) - \langle P_2 \rangle^3 \rangle / \langle (P_2(t) - \langle P_2 \rangle)^2 \rangle^{\frac{3}{2}}$ of the nematic order parameter distribution in the temperature range of the nematic-isotropic transition.

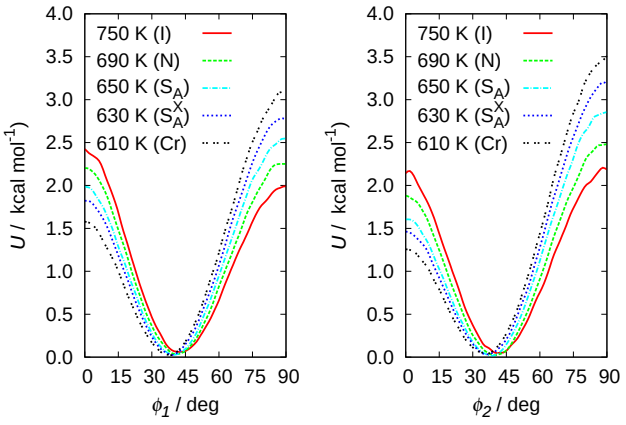

Figure S5: Effective torsional energy profile for the external (ϕ_1 and central (ϕ_2) phenyl-phenyl rotation for selected temperatures corresponding to the different phases.

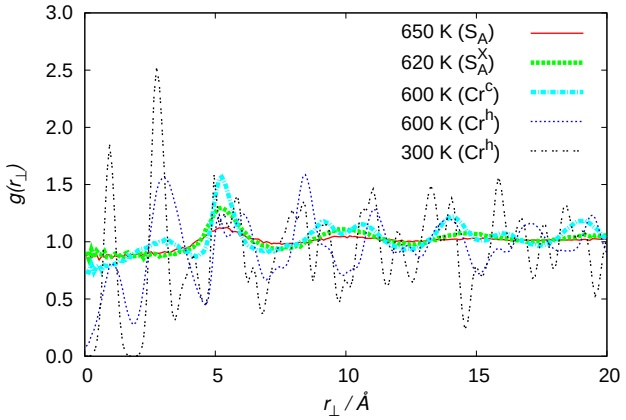

Figure S6: Radial distribution function of the intermolecular distance projected on the plane perpendicular to the phase director. The peaks at $r_\perp < 5$ Å are due to interlayer correlations and appear only in the crystal phase, both in cooling and more pronouncedly in heating runs.

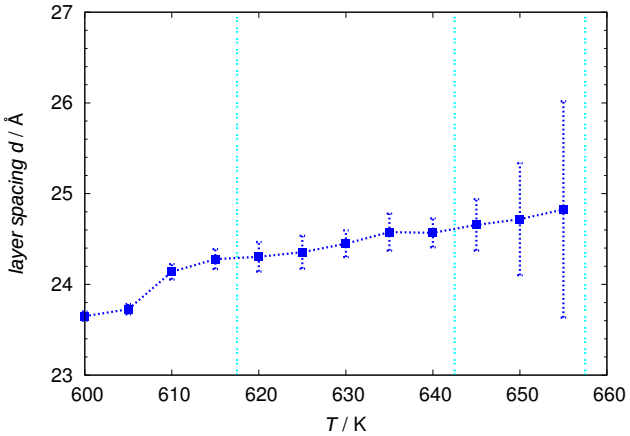

Figure S7: Smectic or crystal layer spacing as a function of temperature for the 1000-molecules sample. Vertical light blue lines indicate the measured transition temperatures.

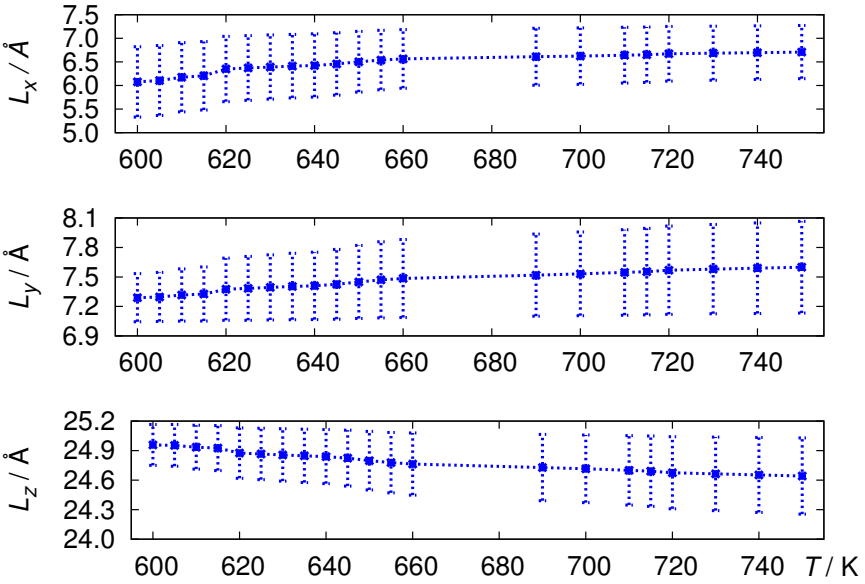

Figure S8: Molecular dimensions along the principal inertial axes as a function of temperature.

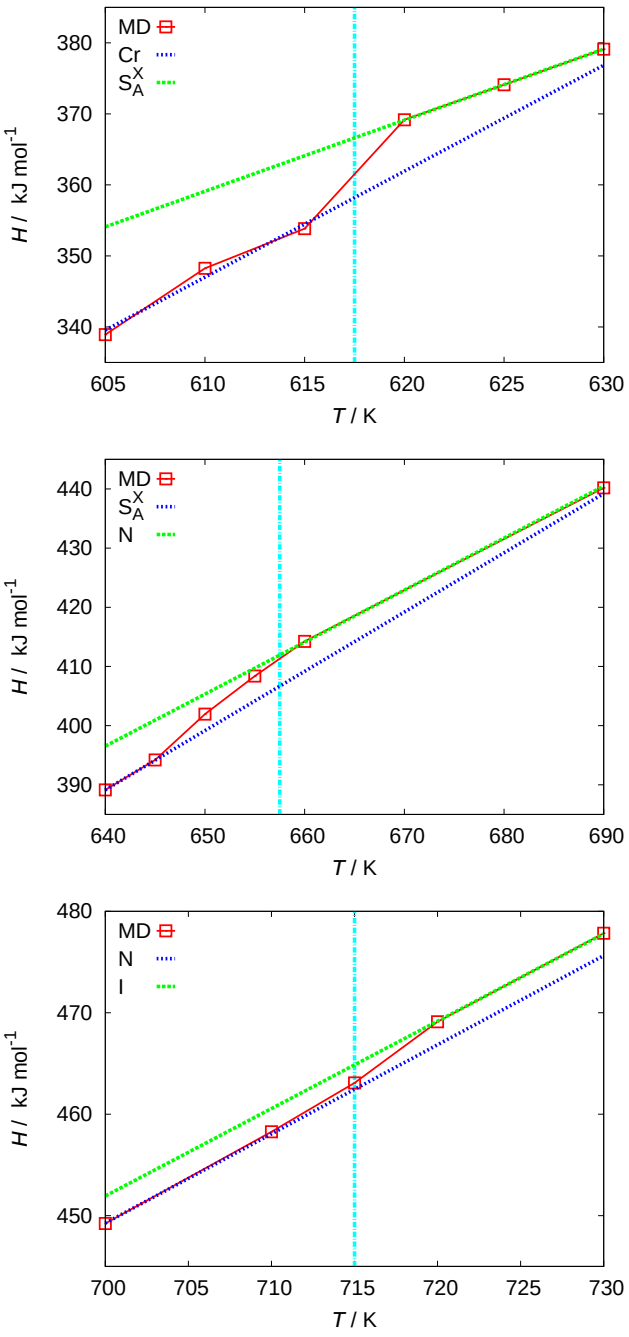

Figure S9: Phase enthalpies interpolated with linear least square fits of the enthalpy in each of the phases. The phase transition enthalpy is estimated as the difference between the two relevant straight lines at the transition temperature (vertical line): from top to bottom, Cr-S_A^X (ΔH=-8.4 kJ·mol^{-1}, ΔS=13.6 J·mol^{-1}·K^{-1} at T=617.5 K), S_A^X-N (ΔH -5.2 kJ·mol^{-1}, ΔS 8.0 J·mol^{-1}·K^{-1} at T=657.5 K), N-I (ΔH=-2.4 kJ·mol^{-1}, ΔS=3.4 J·mol^{-1}·K^{-1} at T=715 K). The S_A phase was neglected as apparently the transitions S_A-N and S_A^X-S_A are of second order.

3 Parameter and topology files in CHARMM format

3.1 Topology file

```
AUTOgenerate ANGLES DIHEDRAL

MASS 1  CA 12.0110  CA
MASS 2  CB 12.0110  CB
MASS 3  CC 12.0110  CC
MASS 4  HA  1.0079  HA


RESIDUE QPH  0.0

*
*       H10     H9    H21    H20     H31   H30    H41   H40    H52   H51
*         C5 - C4       C17-C16       C27-C26      C37-C36      C47-C46
*         /     \       /     \       /     \     /      \     /     \
*  H11- C6       C3 - C12     C15 - C22     C25 - C32    C35 - C42    C45-H50
*         \     /       \     /       \     /      \     /      \     /
*         C1 - C2       C13-C14       C23-C24      C33-C34       C43-C44
*       H7      H8    H18    H19     H28   H29    H38   H39     H48   H49
*

 group
  atom C1     CA -0.130708
  atom C2     CA -0.153622
  atom C3     CB  0.073512
  atom C4     CA -0.153622
  atom C5     CA -0.130708
  atom C6     CA -0.093951
  atom H7     HA  0.120684
  atom H8     HA  0.121869
  atom H9     HA  0.121869
  atom H10    HA  0.120684
  atom H11    HA  0.111224
 group
  atom C12    CB  0.054556
  atom C13    CA -0.153306
  atom C14    CA -0.164759
  atom C15    CC  0.080841
  atom C16    CA -0.164759
  atom C17    CA -0.153306
  atom H18    HA  0.124556
  atom H19    HA  0.125688
  atom H20    HA  0.125688
  atom H21    HA  0.124556
```

```
 group
  atom C22    CC  0.054336
  atom C23    CA -0.154476
  atom C24    CA -0.154476
  atom C25    CC  0.054336
  atom C26    CA -0.154476
  atom C27    CA -0.154476
  atom H28    HA  0.123814
  atom H29    HA  0.123814
  atom H30    HA  0.123814
  atom H31    HA  0.123814
 group
  atom C32    CC  0.080841
  atom C33    CA -0.164759
  atom C34    CA -0.153306
  atom C35    CB  0.054556
  atom C36    CA -0.153306
  atom C37    CA -0.164759
  atom H38    HA  0.125688
  atom H39    HA  0.124556
  atom H40    HA  0.124556
  atom H41    HA  0.125688
 group
  atom C42    CB  0.073512
  atom C43    CA -0.153622
  atom C44    CA -0.130708
  atom C45    CA -0.093951
  atom C46    CA -0.130708
  atom C47    CA -0.153622
  atom H48    HA  0.121869
  atom H49    HA  0.120684
  atom H50    HA  0.111224
  atom H51    HA  0.120684
  atom H52    HA  0.121869

 bond C1  C2      C1  C6      C1  H7      C2  C3      C2  H8
 bond C3  C4      C3  C12     C4  C5      C4  H9      C5  C6
 bond C5  H10     C6  H11     C12 C13     C12 C17     C13 C14
 bond C13 H18     C14 C15     C14 H19     C15 C16     C15 C22
 bond C16 C17     C16 H20     C17 H21     C22 C23     C22 C27
 bond C23 C24     C23 H28     C24 C25     C24 H29     C25 C26
 bond C25 C32     C26 C27     C26 H30     C27 H31     C32 C33
 bond C32 C37     C33 C34     C33 H38     C34 C35     C34 H39
 bond C35 C36     C35 C42     C36 C37     C36 H40     C37 H41
 bond C42 C43     C42 C47     C43 C44     C43 H48     C44 C45
 bond C44 H49     C45 C46     C45 H50     C46 C47     C46 H51
 bond C47 H52

end
```

3.2 Parameter file

```
BOND
CA   CA     478.40    1.400
CA   HA     344.30    1.100
CB   CB     346.50    1.490
CC   CC     346.50    1.480
CA   CB     466.10    1.410
CA   CC     466.10    1.410

ANGLE

CA   CA   CA      67.20   120.00
CA   CA   HA      48.50   120.00
CA   CA   CB      67.20   121.17
CA   CB   CA      67.10   118.65
CA   CC   CA      67.10   118.23
CA   CB   CB      67.20   121.14
CB   CA   HA      48.50   120.00
CC   CA   CA      67.20   121.00
CC   CC   CA      67.20   121.00
CC   CA   HA      67.20   119.40

DIHEDRAL

X    CA   CA   X    3.6250  2 180.
X    CB   CB   X   -0.7048  2   0.
X    CB   CB   X    0.0851  4   0.
X    CB   CB   X   -0.0111  6   0.
X    CB   CB   X   -0.0272  8   0.
X    CB   CB   X   -0.0113 10   0.
X    CC   CC   X   -0.7859  2   0.
X    CC   CC   X    0.0598  4   0.
X    CC   CC   X   -0.0182  6   0.
X    CC   CC   X   -0.0284  8   0.
X    CC   CC   X   -0.0105 10   0.
X    CA   CB   X    3.6250  2 180.
X    CA   CC   X    3.6250  2 180.


NONBONDED

CA 0.   -.1050  1.9080   0.  -.05250  1.9080
HA 0.   -.0150  1.4590   0.  -.00750  1.4590
CB 0.   -.1050  1.9080   0.  -.05250  1.9080
CC 0.   -.1050  1.9080   0.  -.05250  1.9080

END
```

References

[1] J. C. Sancho-Garcìa and J. Cornil. Anchoring the torsional potential of biphenyl at the ab initio level: The role of basis set versus correlation effects. *J. Chem. Theory Comput.*, 1:581–589, 2005.

[2] M. J. Frisch, G. W. Trucks, H. B. Schlegel, G. E. Scuseria, M. A. Robb, J. R. Cheeseman, G. Scalmani, V. Barone, B. Mennucci, G. A. Petersson, H. Nakatsuji, M. Caricato, X. Li, H. P. Hratchian, A. F. Izmaylov, J. Bloino, G. Zheng, J. L. Sonnenberg, M. Hada, M. Ehara, K. Toyota, R. Fukuda, J. Hasegawa, M. Ishida, T. Nakajima, Y. Honda, O. Kitao, H. Nakai, T. Vreven, J. A. Montgomery, Jr., J. E. Peralta, F. Ogliaro, M. Bearpark, J. J. Heyd, E. Brothers, K. N. Kudin, V. N. Staroverov, R. Kobayashi, J. Normand, K. Raghavachari, A. Rendell, J. C. Burant, S. S. Iyengar, J. Tomasi, M. Cossi, N. Rega, J. M. Millam, M. Klene, J. E. Knox, J. B. Cross, V. Bakken, C. Adamo, J. Jaramillo, R. Gomperts, R. E. Stratmann, O. Yazyev, A. J. Austin, R. Cammi, C. Pomelli, J. W. Ochterski, R. L. Martin, K. Morokuma, V. G. Zakrzewski, G. A. Voth, P. Salvador, J. J. Dannenberg, S. Dapprich, A. D. Daniels, Ö. Farkas, J. B. Foresman, J. V. Ortiz, J. Cioslowski, and D. J. Fox. Gaussian 09 Revision D.01. Gaussian Inc. Wallingford CT 2009.

[3] I. Cacelli and G. Prampolini. Torsional barriers and correlations between dihedrals in p-polyphenyls. *J. Phys. Chem. A*, 107:8665–8670, 2003.

[4] J. Hénin, G. Fiorin, C. Chipot, and M. L. Klein. Exploring multidimensional free energy landscapes using time-dependent biases on collective variables. *J. Chem. Theory Comput.*, 6:35–47, 2010.

[5] B. H. Besler, K. M. Merz Jr., and P. A. Kollman. Atomic charges derived from semiempirical methods. *J. Comput. Chem.*, 11:431–439, 1990.

[6] P. A. Irvine, D. C. Wu, and P. J. Flory. Liquid-crystalline transitions in homologous p-phenylenes and their mixtures. part 1.-experimental results. *J. Chem. Soc., Faraday Trans. 1*, 80:1795–1806, 1984.

[7] W. L. Jorgensen, D. S. Maxwell, and J. Tirado-Rives. Development and testing of the opls all-atom force field on conformational energetics and properties of organic liquids. *J. Am. Chem. Soc.*, 118:11225–11236, 1996.

[8] A. Pizzirusso, M. Savini, L. Muccioli, and C. Zannoni. An atomistic simulation of the liquid-crystalline phases of sexithiophene. *J. Mater. Chem.*, 21:125–133, 2011.

[9] C. D. Sherrill, B. G. Sumpter, Mutasem O. Sinnokrot, M. S. Marshall, E. G. Hohenstein, R. C. Walker, and I. R. Gould. Assessment of standard force field models against high-quality ab initio potential curves for prototypes of π-π, CH-π and SH-π interactions. *J. Comput. Chem.*, 30:2187–2193, 2009.

[10] K. N. Baker, A. V. Fratini, T. Resch, H. C. Knachel, W. W. Adams, E. P. Socci, and B. L. Farmer. Crystal structures, phase transitions and energy calculations of poly(p-phenylene) oligomers. *Polymer*, 34:1571–1587, 1993.